Frequency and distribution of winter melt events from passive microwave satellite data in the pan-Arctic, 1988-2013

Libo Wang[1], Peter Toose[1], Ross Brown[2], and Chris Derksen[1]

[1] Climate Processes Section, Climate Research Division, Environment and Climate Change Canada, Toronto, Ontario, Canada

[2] Climate Processes Section, Climate Research Division, Environment and Climate Change Canada@Ouranos, Montreal, Québec, Canada

Correspondence to: Libo Wang (libo.wang@canada.ca)

Abstract

This study presents an algorithm for detecting winter melt events in seasonal snow cover based on temporal variations in the brightness temperature difference between 19 GHz and 37 GHz from satellite passive microwave measurements. An advantage of the passive microwave approach is that it is based on the physical presence of liquid water in the snowpack, which may not be the case with melt events inferred from surface air temperature data. The algorithm is validated using in situ observations from weather stations, snow pit measurements, and a surface-based passive microwave radiometer. The validation results indicate the algorithm has a high success rate for melt durations lasting multiple hours/days and where the melt event is preceded by warm air temperatures. The algorithm does not reliably identify short duration events or events that occur immediately after or before periods with extremely cold air temperatures due to the thermal inertia of the snowpack and/or overpass and resolution limitations of the satellite data. The results of running the algorithm over the pan-Arctic region (north of 50º N) for the 1988-2013 period show that winter melt events are relatively rare totaling less than one week per winter over most areas, with higher numbers of melt days (around two weeks per winter) occurring in more temperate regions of the Arctic (e.g., central Quebec and Labrador, southern Alaska, and Scandinavia). The observed spatial pattern is similar to winter melt events inferred with surface air temperatures from the ERA-interim and MERRA reanalysis datasets. There was little evidence of trends in winter melt event frequency over 1988-2013 with the exception of negative trends over northern Europe attributed to a shortening of the duration of the winter period. The frequency of winter melt events is shown to be strongly correlated to the duration of winter period. This must be taken into account when analyzing trends to avoid generating false positive trends from shifts in the timing of the snow cover season.

1. Introduction

Snow cover is important in Arctic climate and ecological systems and has decreased in areal extent and duration especially during the spring period in response to rapid Arctic warming in recent decades [Brown and Robinson, 2011; Callaghan et al. 2012; Derksen and Brown, 2012]. The conventional wisdom is that Arctic warming will result in an increase in the frequency and duration of winter melt events, which may also include rain-on-snow (ROS) events. These winter melt/refreeze events modify the physical properties of snow (albedo, density, grain size, thermal conductivity), generate winter runoff [Bulygina et al., 2010; Johansson et al., 2011] and can result in potentially significant impacts on the surface energy budget, hydrology and soil thermal regime [Boon et al., 2003; Hay and McCabe, 2010; Rennert et al., 2009]. The refreezing of melt water can also create ice layers that adversely impact the ability of ungulate travel and foraging

[Hansen et al., 2011; Grenfell and Putkonen, 2008], and exert uncertainties in snow mass retrieval from passive microwave satellite data [Derksen et al., 2014; Rees et al., 2010]. Winter warming and melt events may also damage shrub species and tree roots, affecting plant phenology and reproduction in the Arctic [AMAP, 2011; Bokhorst et al., 2009].

Winter melt events are rare extreme events over most of the Arctic and are sporadic in time and space [Pedersen et al., 2015]. These events are linked to intrusion of warm air from southerly or southwesterly flow, may be associated with fog [Semmens et al. 2013], rain and/or freezing rain, and typically last for several days. Previous studies [Cohen et al. 2015; Rennert et al 2009] have shown that the synoptic conditions associated with these events are closely related to larger modes of atmospheric circulation.

Microwave remote sensing measurements are very sensitive to the presence of liquid water in snow. Dry snow is a mixture of air and ice. Because the permittivity of water is much higher than air and ice at microwave frequencies, the introduction of even a small amount of liquid water (0.5 %) in snow can increase the permittivity of snow by over an order of magnitude [Ulaby et al., 1986]. This increases absorption and reduces the penetration depth, which in turn results in a large increase in brightness temperature (T_B) and decrease in radar backscatter. Satellite active and passive microwave measurements have been widely used for snow melt detection over various components of the Arctic cryosphere during the spring melt period [e.g., Kim et al., 2011; Markus et al., 2009; Tedesco, 2007; Wang et al., 2011]. Only a few satellite studies have focused on winter melt or ROS detection, and are mainly for specific regions or limited time periods [Bartsch, 2010; Bartsch et al., 2010; Doland et al., 2016; Grenfell and Putkonen, 2008; Semmens et al., 2013; Wilson et al., 2012]. Here we develop an algorithm to detect winter melt from satellite passive microwave (PMW) data over pan-Arctic snow-covered land areas north of 50º N for the period 1988-2013.

Winter melt and ROS events can also be inferred from surface weather observations [Groisman et al., 2003; McBean et al., 2005; Pedersen et al., 2015], reanalyses [Cohen et al. 2015; Rennert et al., 2009], or reanalysis-driven snowpack models [Liston and Hiemstra, 2010]. In most of these studies, winter melt events are assumed to occur when the daily surface air temperature exceeds a certain threshold. For example, Groisman et al. [2003] defined a thaw day as a day with snow on the ground when the daily mean surface air temperature is above -2º C. Inferring thaw events from surface air temperatures in this way does not consider the energy balance of the snowpack. In addition, reanalysis datasets can contain important biases and inhomogeneities over the Arctic [e.g. Rapaic et al. 2015] that will impact the spatial and temporal frequency of the inferred winter thaw events. The advantage of the passive microwave approach described above is that melt events are directly linked to the appearance of liquid water in snow which drives changes in snowpack properties relevant to Arctic ecosystems. The brightness temperature time series is also considered to be consistent over the 1988-2013 period as it is derived from near identical spaceborne sensors.

Previous studies have linked field observations of ice layer formation from ROS events with satellite measurements [Bartsch et al., 2010; Grenfell and Putkonen, 2008], but few studies have showed links between satellite measurements and in situ observations of changes in snow properties from melt/refreeze events [Langlois et al., 2012; Nghiem et al., 2014]. Passive microwave satellite data have two important limitations for detecting melt/refreeze events: the relatively coarse resolution (10-25 km) and the twice daily overpasses. Thus melt events of short duration or limited spatial distribution may not be detectable. The objectives of this study are to (1) develop an algorithm for winter melt detection from PMW data, and (2) to characterize winter melt events detectable by PMW at the satellite scale using weather station observations, surface–based PMW radiometer measurements, and snowpit surveys observed during multiple field campaigns. These PMW results are compared to winter melt detection results inferred from near surface air temperature fields from two commonly used reanalysis datasets. Trends in PMW-derived winter melt frequency over the period 1988-2013 are presented along with a demonstration of the impact on trend results of using a fixed winter period for defining the snow season.

2. Data and Methods

2.1. Satellite passive microwave data

This study uses T_B data from the Special Sensor Microwave/Imager (SSM/I, 1987–2008), and the Special Sensor Microwave Imager/Sounder (SSMIS, 2009 to present) re-projected to 25 km equal-area scalable earth-grid (EASE-Grid) available from the National Snow and Ice Data Center in Boulder, Colorado [Armstrong et al., 1994]. These sensors provide a continuous time series of T_B since 1987 (Table 1). We do not perform sensor cross calibration given that only small differences were found between sensors [Abdalati et al., 1995; Cavalieri et al., 2012; Stroeve et al., 1998]. Since our melt detection algorithm (described below) only uses the relative change in the temporal variations in T_B, slight offsets in absolute T_B between sensors should not affect algorithm performance. The gaps in the data are filled by linear interpolation from adjacent days. Vertically polarized T_B from both morning and afternoon overpasses are utilized to increase the likelihood of observing melt events. Due to large temporal gaps in the early SSM/I record, the time series used begin in the fall of 1988 and extend to 2014 (Table 1). Although horizontal polarized measurements are more sensitive to ice lenses within the snowpack [Derksen et al., 2009; Rees et al., 2010], there is not much difference between the two polarizations for melt detection and we use vertically polarized measurements to be consistent with Wang et al. [2013].

2.2. Winter melt detection method for PMW

As the purpose of this study is to detect winter melt events, the winter period duration (WPD) is defined as occurring between the main snow onset date (MSOD) in the fall (beginning of continuous dry snow cover on the ground) and the main melt onset date (MMOD) in the spring (i.e. the beginning of the period with frequent melt/freeze diurnal cycles) at each pixel. Figure 1 illustrates the steps involved in detecting melt events for the WPD, based on the temporal variations in the difference of the brightness temperature (T_BD) between 19 GHz and 37 GHz and a 37 GHz T_B threshold. For dry snow conditions, as snow accumulates T_BD increases due to the larger scattering effect of the microwave signal by snow grains at 37 GHz versus 19 GHz [Chang et al., 1987]. Upon the appearance of liquid water in snow, T_B increases at both frequencies and results in a sharp drop in T_BD, to similar magnitudes seen in snow free conditions, but will quickly revert back to dry snow T_BD levels once the snow refreezes allowing for the detection of melt/refreeze events (Figure 2).

The purpose of determining MSOD is to capture the earliest start date of the continuous dry snowpack. The MSOD is determined as the first date when (1) $T_BD \geq Tsn$ (a threshold = mean July T_BD + 3.5 K) for 7 out of 10 days and (2) $T_B37v < 253$ K for 10 out of 11 days (Figure 1). The thresholds and conditions were optimized by comparing the PMW determined MSOD to daily snow depth observations from the Global Surface Summary of the Day dataset archived at the National Climate Data Center (http://www.ncdc.noaa.gov). The T_B criterion in (2) is applied to exclude periods with T_BD fluctuations related to early season freeze/thaw cycles rather than winter melt events (see below for its derivation).

MMOD is determined following Wang et al. [2013]. Their algorithm was based on temporal variations in T_BD relative to the previous 3-day average T_BD (referred as M hereafter). Melt onset was detected if the difference in M and daily T_BD was greater than a threshold (TH_{old}= 0.35*M) for four or more consecutive days. Based on trial and error, the MMOD detection algorithm in Wang et al [2013] is modified here to detect mid-winter melt events that are typically of shorter duration. Firstly, the threshold is modified slightly from TH_{old} = 0.35*M to TH_{new} = 0.4* M (pixel-dependent) since the goal is to detect melt events with one or more days of duration (instead of four or more days as in the previous study), and secondly, a T_B37v threshold condition is added following Semmens et al. [2013] to mitigate false detection due to T_BD changes not related to melt (e.g., from noise or artifacts from data gap filling). The resulting expression for winter melt event conditions is $(M-T_BD) > TH_{new}$ and $T_B37v \geq 253$ K for one day

(Figure 1), referred as the winter T_BD algorithm hereafter. The $T_B37v \geqslant 253$ K condition was obtained by evaluating a range of T_B37v values from 250-255 K, at 1 K increments to identify the threshold most sensitive to the presence/absence of liquid water in snow. This was inferred from histograms of daily maximum (Tmax), mean (Tm), and minimum (Tmin) air temperatures for days detected as melting at all available weather stations during 2000-2007 (see locations in Figure 5b, ~5100 observations in total). The results show that for $T_B37v = 253$ K, Tmax is ⩾ 0º C for nearly 96% of cases, Tmin is < 0º C for 94%, and Tm is ⩾ 0º C for 80%. This suggests that the PMW-detected winter melt events are consistent with diurnal positive air temperature events, while most of the events (80%) probably last multiple hours thus corresponding to days with Tm⩾ 0º C. If a melt event is detected within 10 days from the MMOD, then it is not considered a mid-winter melt event, but rather a preliminary melt event to the MMOD and is excluded from the analysis.

An example of the performance of the winter T_BD algorithm is shown in Figure 2 for a case at Pudasjarvi, Finland (65.4º N, 26.97º E) during the 2013- 2014 winter. At Pudasjarvi station, the snow depth first became greater than 0 cm on day of year (DOY) 291 of 2013. The snow depth was mostly less than 10 cm for days 291 to 332, with two periods of no snow on the ground while Tmax fluctuated around 0º C. The PMW detected MSOD was on DOY332, corresponding within one week of the date of continuous snow cover above 10 cm observed at the station (Figure 2b). MMOD was detected on DOY64 of 2014, however, there was still snow on the ground until DOY108, typical of high latitude snow cover where melt onset is followed by the spring thaw, which is a sustained period with high diurnal air temperature variation where the snowpack is melting during the day and refreezing at night. At the end of this melt–refreeze period, the snowpack may be actively melting both day and night until snow disappearance, which can take several weeks [Semmens et al., 2013]. During winter 2013-2014, 20 melt days in total were detected at Pudasjarvi, all corresponding to days with Tmax $\geqslant 0^{o}$ C. However, not all days with Tmax $\geqslant 0^{o}$ C are detected by PMW as melting, for example DOY351-352, for reasons which will be explained further in the validation section.

The winter T_BD algorithm is applied to time series of T_B for each winter over the period 1988-2013. Melt events may last from one to several days and in some cases the algorithm may split events. For this reason we use the annual number of melt days (rather than number of events) in presenting and analyzing the results. The WPD varies at each pixel and is determined by MSOD and MMOD as described above. This approach is referred to as "PMW-varying" in the following analysis. Since we focus on melt events during the winter period, the T_BD algorithm is only applied to pixels with MSOD detected before the end of December and with MMOD later than March 1st, i.e. with WPD > 60 days. The PMW-varying approach is internally consistent in that it takes account of annual variations in winter temperature and snow cover. This is not the case for analysis using a fixed "winter" window where spurious trends can be created from changing seasonality (i.e. earlier snow melt). To highlight this, a fixed window approach is also applied ("PMW-fixed") where the T_BD algorithm is applied to time series of T_B from November to April. The results presented in the following sections are from the PMW-varying method unless explicitly indicated otherwise. Since the microwave response of melt on permanent snow and ice is different from seasonal terrestrial snow cover, we mask out the Greenland Ice sheet and glaciers in our analyses.

2.3. Winter melt detection for reanalysis datasets

Winter melt event information from the 0.75º x 0.75º latitude/longitude European Centre for Medium-Range Weather Forecasts Re-Analysis Interim (ERA-I) [Dee et al., 2011] and the 1/2º latitude by 2/3º longitude Modern Era-Retrospective Analysis for Research and Applications (MERRA) [Rienecker et al 2011] reanalyses were used to evaluate the melt event climatology generated by the PMW method. Melt events in the reanalyses are inferred from 6-hourly air temperatures over the same period as the satellite data. For the comparison, a winter thaw event is defined as a period of above-freezing daily mean air temperature occurring during the winter period dominated by below-freezing air temperatures. Here the winter period is defined by 0° C crossing dates (between fall and spring) obtained with a centered 30-day moving average of daily mean air temperature, which is analogous to the "PMW-varying" method described above. An additional condition is imposed of a surface snow cover of at least 10 cm depth for ERA-I and 4 mm SWE for MERRA to obtain results comparable to the PMW method of detection over snow covered ground. The mean daily air temperature is the average of the 00, 06, 12 and 18 UTC values. Snow depths for ERA-I are taken from the daily snow depth reconstruction described in Brown and Derksen [2013] to avoid various inconsistencies with the snow depths in the reanalysis.

2.4. In situ field observations and methods

The satellite-based winter T_BD algorithm is validated with surface–based PMW radiometer measurements along with near surface air/snow temperature observations recorded on April 12th-13th, 2010 during a field campaign near Churchill, Manitoba, Canada [Derksen et al., 2012]. A modified version of the winter T_BD algorithm is applied to the surface-based radiometer measurements due to the continuous nature of the data. We simply used the average T_B values from the stable pre-melt period as our reference frozen T_BD value instead of previous 3-day average.

Furthermore, we try to characterize winter melt events detectable by the winter T_BD algorithm using snowpit surveys recorded during multiple PMW snow measurement campaigns conducted between 2005 and 2010 in both the boreal forest and tundra environments of Canada (Table 2). The number of satellite detected melt events for the specific EASE-Grid pixels surrounding the snow pit locations are compared to the number of melt forms/ice formations identified within the snowpack. A melt feature identified lower (closer to the ground) is consider an early winter event, while those melt features identified closer to the surface of the snow are considered more recent events. An example of the coincident satellite, air temperature and snow pit information for a survey site near Thompson, Manitoba is shown in Figure 3. Hourly air temperatures from weather stations in the vicinity of the snow pits (within 70 km), are examined to identify if and when a melt event occurred in the region, how long the melt event lasted, what the average temperature was for the duration of the event and what the minimum, maximum and average 36 hour air temperatures were preceding the melt event. Results of the field evaluation are presented in Section 3.1

2.5. Other data and analysis methods

Gridded (5º x 5º) monthly surface air temperature over land areas during the study period are obtained from the Climatic Research Unit (University of East Anglia) CRUTem4 dataset [Jones et al., 2012]. Seasonal air temperature trends for the fall (September – November), winter (December – February), and spring (March – May) periods are computed to assist the interpretation of trends in winter melt events. The Mann-Kendall method is used for trend analysis taking into account serial correlation following Zhang et al. [2000]. Trends are only computed at grid cells with melt events detected in at least 12 winters, and grid cells with trends statistically significant at 90% level are shown. Correlations between the winter melt related variables are computed using the Pearson's correlation method with significance levels determined from the two-tailed Student's *t* test.

3. Results

3.1. Field evaluation of the winter T_BD algorithm

Figure 4 illustrates the time series of the surface-based radiometer T_B and air/snow temperature measurements recorded during the April 12th-13th melt event near Churchill. The area shaded in green highlights the period for which the modified T_BD algorithm identified the melt event. As the near surface air temperatures approached 0º C, T_B increased rapidly at both the 19 and 37 GHz. The detected melt onset occurred ~ 40 minutes after the 11 cm and 7 cm air temperatures crossed the 0° C threshold and 25 minutes before the 2 m air temperature exceeded 0° C, likely due to radiant heating from the sun to the snow surface and the boundary layer air temperature probe. The -1 cm snow temperature did not reach 0° C until three hours after the detected melt onset, suggesting that the rapid increases in T_B here were responses to the appearance of liquid water in the snow surface. The influence of radiant heating is evident during the late afternoon/early evening as the incoming solar radiation lessens as the sun begins to set (~1900 h local), at which point the snowpack and boundary layer air temperatures all drop below 0° C, coinciding with a decrease in T_B even while the 2 m air temperatures are still positive. Compared to the rapid increase in T_B during the melt onset, the more gradual decrease in T_B is likely due to the mixed effects of uneven re-freezing of the snow surface and delayed freezing of sub-surface liquid water.

The validation results from the seven snowpit survey sites and twelve melt events are summarized in Table 2. The performance of the winter T_BD algorithm is highlighted in bold for a successful melt detection and in italic for a failed detection. The results suggest that a successful detection is likely when the melt duration lasts for periods longer than six hours and/or the melt event has been preceded by warm air temperatures that have warmed the snowpack to near melting conditions (previous day's Tmax > -3° C). In these situations, it is common for melt features to form within the snowpack. The algorithm does not reliably identify short duration melt events or events that occur immediately after extremely cold air/snowpack temperatures (previous 36 hour minimum air temperature < -13° C). In these instances, the snowpack likely has enough thermal inertia to remain within a frozen state for the whole duration of the melt event, or very quickly return to a frozen state and thus liquid water is not detectable with satellite T_B. Out of all twelve melt events investigated, six events coincided with observed ROS. Of the six ROS events, half were associated with successful satellite melt detection. Those ROS events that were successfully detected were followed by a continued warming of air temperatures that likely delayed the refreezing of the liquid water in the snow. Those ROS events that were not detected fall under the category of a short duration melt event as described above.

The winter T_BD algorithm is very sensitive to liquid water within the snow, but does not necessarily capture all events that can create melt features within the snowpack, largely due to the fact that liquid water from both melt and ROS events tends to re-freeze quickly during the winter months and unless these events occur very close to the timing of the satellite overpass (ascending ~ 1830 h and descending 0630 h local time), they may remain undetected. In addition, wide-spread, spatially expansive melt or ROS events are rare [Bartsch, 2010; Cohen et al., 2015], and as such may be missed by the coarse resolution (25 km) PMW data. These limitations are common to other melt detection techniques that utilize current spaceborne passive microwave sensors.

3.2. The spatial distribution of winter melt events

Figure 5 shows the PMW-derived MSOD, MMOD, and WPD during the 1988-2013 period. On average, continuous snow cover starts in the Canadian Arctic islands and high elevation regions of the Arctic in September and progresses to the open tundra in October (Figure 5a). By November, most of the areas north of 50º N are covered by snow except for some temperate maritime and lower latitude regions where continuous snow cover sets in December. The spring main melt onset starts at lower latitudes in March, progresses to the boreal forests and tundra in April/May, and reaches the high Arctic in June (Figure 5b), giving rise to spatial variability in the duration of the winter period from one to seven months on average (Figure 5c). A pixel-wise definition of winter period for melt detection is required to account for this spatial variability as well as the temporal variability from year-to-year fluctuations in snow cover.

During the 26 winters covered by this study, melt occurred at least once everywhere north of 50º N using the PMW-varying window method (Figure 6a). However, the average cumulative number of melt days is less than one week per winter for most areas, with more melt days (around two weeks per winter) occurring in areas with a relatively long snow season and more temperate winter climates (e.g., central Quebec and Labrador, southern Alaska, and Scandinavia). The spatial distribution patterns of NMD from ERA-I (Figure 6c) and MERRA (Figure 6d) generally agree with that from PMW. However, ERA-I detects about one week more melt days on average in most areas , while MERRA detects less melt days in Quebec and central Canada relative to PMW. Both ERA-I and MERRA detect more melt days in southern Alaska and western North America (NA). These are relatively deep snowpack regions where melt may not occur in short periods of freezing air temperatures due to the thermal inertia of the snowpack. Compared to the PMW-varying window method (Figure 6a), there are many more melt days detected using the PMW-fixed window method (Figure 6b), especially in the relatively temperate climate regions (e.g., northern Europe and lower latitudes of NA and Russia) where the WPD is relatively short and thus limits the possible number of melt days to be detected.

Figure 7 shows the monthly mean NMD from October to June during the period 1988-2013. Winter melt events mainly occur in the fall (October-November) and spring (April-June) months at high latitudes (>60º N) where continuous snow starts early and melts late (Figure 5). During November to March for the period 1988-2013, no winter melt events are detected across large areas of Siberia and the Canadian and the Alaskan tundra where the monthly surface air temperature is usually lower than -20º C (not shown). On average, April has the maximum extent and duration of winter melt events (Figure 7).

3.3. Changes in snow cover and winter melt events

The PMW-derived estimates of changes in snow cover (MSOD, MMOD, and WPD) over the 1983-2013 period are shown in Figure 8. Large regions of the Arctic exhibits trends to later snow onset, particularly over northern Scandinavia, western Russia, Alaska, and Quebec (Figures 8a and 8d). The timing of the spring main melt onset date exhibits trends to earlier melt over most of the Arctic except for northern Europe and western NA (Figures 8b and 8e). The net effect is significant negative trends in winter duration period that exceed -10 days/decade over large regions of the Arctic (Figures 8c and 8f).

Over the study period, there are few significant trends in NMD over the Arctic (Figures 9a and 9c), and where there are significant trends, these are dominated by decreases over northern Europe. The spatial distribution patterns of NMD trends contrast markedly between the PMW-varying and the PMW-fixed results (Figures 9b and 9d). Trends from PMW-fixed are dominated by increasing trends in NMD over most of the Arctic except for northern Europe. Corresponding trends from the reanalyses are not shown because the annual winter thaw frequency series from ERA-I and MERRA are not always consistent over the 1988-2013 period in some regions. For example over northern Quebec (not shown) the two series are well correlated over the period from 1980-2001 ($r=0.75$, $p < 0.001$) but diverge markedly after 2001 when numerous changes in data assimilation streams occurred in both reanalysis datasets [Rapaic et al. 2015]. This underscores the advantage of the PMW melt detection approach which is based on a consistent T_B time series.

4. Discussion and conclusions

An algorithm for detecting terrestrial winter melt events using satellite PMW measurements is developed and evaluated using in situ observations at weather stations and field surveys. The winter T_BD algorithm is able to successfully detect winter melt events lasting for more than six hours in different environments but is less successful for short duration melt and ROS events due to the thermal inertia of the snowpack and/or the overpass and resolution limitation of the PMW data. The algorithm should also be able to detect subsurface melt events although this aspect was not evaluated in this paper. Similar channel difference approaches have also been used for melt onset detection over the Arctic sea ice [e.g., Drobot and Anderson, 2001]. However, the emissivities of first-year sea ice are different than that of multiyear sea ice, and the emissivities over multiyear sea ice can have a large range due to the varied histories of the ice floes. These complicate the detection of melt over sea ice, so we do not recommend the use of the algorithm developed in this study for melt detection over sea ice. A multiple indicators approach was developed in Markus et al. [2009] for melt/refreeze detection over the Arctic sea ice.

During the period 1988-2013, winter melt occurred at least once everywhere north of 50º N. The average cumulative melt days totaled less than one week per winter for most Arctic areas, with more melt days (approximately two weeks per winter) occurring in areas with relatively long snow season and temperate climate. Winter melt events are not detected in some areas of Siberia and the Canadian and the Alaskan tundra where the monthly SAT is usually lower than -20º C. The spatial distribution patterns of NMD are in general consistent with results inferred from surface air temperature data in the reanalysis datasets (ERA-I and MERRA) and PMW, and also with the spatial patterns of refreeze events derived from QuikSCAT for north of 60º N [Bartsch, 2010; Bartsch et al., 2010].

Over the period 1988-2013, large regions of the Arctic exhibit trends to later snow onset in fall and earlier melt onset in spring, resulting in significant negative trends in winter period duration. The number of melt days was observed to be significantly positively correlated with the duration of winter period over most of the Arctic, particularly in regions where interannual variability in snow cover is higher (Figure 10). However, there are few areas of the Arctic with locally significant trends in NMD except for northern Europe, where there is evidence of significant negative NMD trends consistent with the positive correlations between WPD and NMD over this area (as shown in Figure 10). The lack of significant trends in winter melt events observed in this study is considered to be related to the relatively short period of data available for analysis and the dynamic mechanisms generating winter melt and ROS events that produce more random and chaotic environmental response patterns [Trenberth et al. 2015; Cohen et al. 2015]. This is underscored by trend analysis of annual numbers of winter melt events in ERA-I and MERRA over a longer 1980-2014 period (not shown) where locally significant increasing trends were only observed at 1% of snow covered land points in MERRA and 2% in ERA-I. Cohen et al [2015] also found that the frequency of ROS events was correlated to large-scale modes of atmospheric circulation that contributes to regional-scale variability in ROS trends. The absence of positive winter melt trends observed in this study may also be linked to the seasonal pattern of warming over Arctic land areas during 1988-2013, which is dominated by warming in the snow cover onset fall period (trend=0.67°C/decade, $p<0.001$) with comparatively little warming in the winter (trend=-0,15°C/decade, p=0.47) and spring (trend=0.20°C/decade, p=0.22) period. The spatial character of winter warming over the period (Fig. 11) also shows little warming or cooling over the regions experiencing the largest NMD frequencies. This conclusion is consistent with the findings of Cohen et al. [2012].

There is field evidence of changes in snowpack density and ice layers from a number of locations in the Arctic that is supported by an increased frequency of winter thaw events [Chen et al., 2013; Groisman et al., 2003; McBean et al., 2005; Johansson et al., 2011]. However, winter thaw events in some of these studies were inferred from air temperature observations [Groisman et al., 2003; McBean et al., 2005], which are different from results detected by PMW measurements. As previously pointed out in Figure 9b, the frequency of winter melt events is strongly influenced by the method used to define WPD. A spatially and temporally varying definition of WPD is required as the use of a fixed window generates artificial NMD trends from changes in the timing of the snow cover season. This is further demonstrated in Figure 12 where monthly NMD trends are computed using a fixed WPD of November-April. The results clearly demonstrate that increases in NMD are being driven by trends during the snow cover shoulder seasons of November-December and March-April and not the main winter period. A number of studies reporting increasing NMD trends used fixed winter periods in their analyses [e.g., Groisman et al., 2003; McBean et al., 2005].

The major advantage of the PMW winter melt event method presented here is that it is based on physical processes in the snowpack (melt/freeze), unlike thaw events inferred from air temperature observations that may or may not be associated with snowpack melt processes depending on the thermal inertia of the snowpack. The PMW series is also consistent over time unlike some reanalysis datasets. Several studies have focused on the development of ROS detection methods using PMW data and encouraging results were obtained at some field sites [e.g., Doland et al., 2016; Grenfell and Putkonen, 2008; Langlois et al., 2016]. Future work will focus on the detection of pan-Arctic ice lenses (from both melt/refreeze and ROS events) by integrating PMW techniques. Additional work is also needed to evaluate the performance of the winter melt algorithm in areas with deep snow and complex terrain where the range in T_BD for dry snow versus wet snow is likely to be much smaller [Tong et al., 2010].

Acknowledgements. The In-situ snow survey data used in this study are the result of multiple campaigns carried out over many years and supported by numerous organizations who have provided direct funding, logistical support, or contributed people in the field. There are too many individuals involved to list here, but we would like to acknowledge the institutions and funding sources that contributed to this effort: Environment and Climate Change Canada, the Canadian Space Agency, University of Waterloo, Université de Sherbrooke, Wilfrid Laurier University, the Churchill Northern Study Centre, the Aurora Research Institute, the Canadian Foundation for Climate and Atmospheric Science, Manitoba Hydro, the Northwest Territories Power Corporation and Indian and Northern Affairs Canada. The following data centers are acknowledged for providing data: The National Snow and Ice Data Center for passive microwave satellite data, the National Climate Data Center for the Global Summary of the Day dataset, the Climatic Research Unit - University of East Anglia for the CRUtem4v gridded air temperature data, the European Centre for Medium-Range Weather Forecasts (ECMWF) for the ERA-interim data, and the Global Modeling and Assimilation Office (GMAO) at NASA

Goddard Space Flight Center for MERRA data. The authors would like to thank Anne Walker for providing helpful comments to an early version of the manuscript.

References

Abdalati, W., Steffen, K., Otto, C., and Jezek, K. C.: Comparison of brightness temperatures from SSM/I instruments on the DMSP F8 and F11 satellites for Antarctica and the Greenland ice sheet, Int. J. Remote Sens., 16, 1223–1229, doi:10.1080/01431169508954473, 1995.

AMAP: Snow, Water, Ice and Permafrost in the Arctic (SWIPA): Climate Change and the Cryosphere, Arctic Monitoring and Assessment Programme (AMAP), Oslo, Norway, xii + 538pp, 2011.

Armstrong, R. L., Knowles, K. W., Brodzik, M. J., and Hardman, M. A.: DMSP SSM/I Pathfinder Daily EASE-Grid Brightness Temperatures (1988–2013), Boulder, Colorado, USA, National Snow and Ice Data Center, 1994.

Bartsch, A.: Ten Years of SeaWinds on QuikSCAT for Snow Applications, Remote Sens., 2, 1142-1156; doi:10.3390/rs2041142, 2010.

Bartsch, A., Kumpula, T., Forbes, B. C., and Stammler, F.: Detection of snow surface thawing and refreezing in the Eurasian Arctic with QuikSCAT: implications for reindeer herding, Ecol. Appl., 20, 2346–2358, 2010.

Bokhorst, S. F., Bjerke, J. W., Tømmervik, H., Callaghan, T. V, and Phoenix, G. K.: Winter warming events damage sub - Arctic vegetation: Consistent evidence from an experimental manipulation and a natural event, J. Ecol., 97, 1408-1415, 2009.

Boon, S., Sharp, M., and Nienow, P.: Impact of an extreme melt event on the runoff and hydrology of a high Arctic glacier, Hydrol. Process., 17, doi: 10.1002/hyp.1194, 2003.

Brown, R. D. and Robinson, D. A.: Northern Hemisphere spring snow cover variability and change over 1922–2010 including an assessment of uncertainty, The Cryosphere, 5, 219-229, doi:10.5194/tc-5-219-2011, 2011.

Brown, R. and Lemay, M.: Climate variability and change in the Canadian Eastern Subarctic IRIS region (Nunavik and Nunatsiavut), Chapter 2 in: Allard, M. and M. Lemay (Eds), Nunavik and Nunatsiavut: From science to policy, An Integrated Regional Impact Study (IRIS) of climate change and modernization, Arctic Net Inc., Quebec City, Canada, 303p, 2012.

Brown, R. D. and Derksen, C.: Is Eurasian October snow cover extent increasing? Environ. Res. Lett., 8, 024006, doi:10.1088/1748-9326/8/2/024006, 2013.

Bulygina, O. N., Groisman, P. Y., Razuvaev, V. N., and Radionov, V. F.: Snow cover basal ice layer changes over Northern Eurasia since 1966, Environ. Res. Lett., 5, 015004, doi: 10.1088/1748-9326/5/1/015004, 2010.

Callaghan, T.V., Johansson, M., Brown, R. D., Groisman, P. Y., Labba, N., Radionov, V., Barry, R. G., Bulygina, O. N., Essery, R. L., Frolov, D. M., and Golubev, V. N.: The changing face of Arctic snow cover: A synthesis of observed and projected changes, Ambio, 40, 17-31, 2011.

Chang, A., Foster, J., and Hall, D.: Nimbus-7 SMMR derived global snow cover parameters, Ann. Glaciol., 9, 39– 44, 1987.

Cavalieri, D. J., Parkinson, C., DiGirolamo, N., Ivanoff, A.: Intersensor Calibration Between F13 SSMI and F17 SSMIS for Global Sea Ice Data Records, NASA technical report, 13pp, 2012.

Chen, W., Russell, D. E., Gunn, A., Croft, B., Chen, W. R., Fernandes, R., Zhao H., et al.: Monitoring habitat condition changes during winter and pre-calving migration for Bathurst Caribou in northern Canada, Biodivers., 14, 36-44, 2013.

Cohen, J., Ye, H. and Jones, J.: Trends and variability in rain-on-snow events, Geophys. Res. Lett., 42, 7115-7122, 2015.

Cohen, J., Furtado, J., Barlow, M., Alexeev, V., and Cherry, J.: Asymmetric seasonal temperature trends, Geophys. Res. Lett., 39, doi:10.1029/2011GL050582, 2012.

Dee, D. P., Uppala, S. M., Simmons, A. J., Berrisford, P., Poli, P., Kobayashi,S., … Vitart, F.: The ERA-Interim reanalysis: Configuration and performance of the data assimilation system, Q. J. R. Meteorol. Soc., 137, 553–597, doi:10.1002/qj.828, 2011.

Derksen, C., Sturm, M., Liston, G., Holmgren, J., Huntington, H., Silis, A., et al.: Northwest Territories and Nunavut snow characteristics from a sub-Arctic traverse: Implications for passive microwave remote sensing, J. Hydrometeorol., 10, 448–463, 2009.

Derksen, C., Toose, P., Lemmetyinen, J., Pulliainen, J., Langlois, A., Rutter, N., Fuller, M. C.: Evaluation of passive microwave brightness temperature simulations and snow water equivalent retrievals through a winter season, Remote Sens. Environ., 117, 236-248, 2012.

Derksen, C., Lemmetyinen, J., Toose, P., Silis, A., Pulliainen, J., Sturm, M.: Physical properties of Arctic versus subarctic snow: Implications for high latitude passive microwave snow water equivalent retrievals, J. Geophys. Res., 119, 7254–7270, doi:10.1002/2013JD021264, 2014.

Drobot, S. D., and Anderson, M. R.: An improved method for determining snowmelt onset dates over Arctic sea ice using scanning multichannel microwave radiometer and Special Sensor Microwave/ Imager data, J. Geophys. Res., 106, 24,033 – 24,049, doi:10.1029/2000JD000171, 2001.

Dolant, C., Langlois, A., Montpetit, B., Brucker, L., Roy, A., and Royer, A.: Development of a rain-on-snow detection algorithm using passive microwave radiometry, Hydrol. Process., 30: 3184–3196. doi: 10.1002/hyp.10828, 2016.

Grenfell, T. C. and Putkonen, J.: A method for the detection of the severe rain-on-snow event on Banks Island, October 2003, using passive microwave remote sensing, Water Resour. Res., 44 W03425, 2008.

Groisman, P. Y., Sun, B., Vose, R. S., Lawrimore, J. H., Whitfield, P. H., Førland, E., Hanssen-Bauer, I., Serreze, M. C., Razuvaev, V. N. and Alekseev, G. V.: Contemporary climate changes in high latitudes of the Northern Hemisphere: daily time resolution, Proc. 14th AMS Symp. on Global Change and Climate, 1-10, 2003.

Hansen, B. B., Aanes, R., Herfindal, I., Kohler, J. and Saether, B. E.: Climate, icing, and wild arctic reindeer: past relationships and future prospects, Ecology, 92, 1917–23, 2011.

Hay, L. E. and McCabe, G. J.: Hydrologic effects of climate change in the Yukon River Basin, Clim. Chang., 100, 509-523, 2010.

Johansson, C., Pohjola, V. A., Jonasson, C., and Callaghan, T.V.: Multi-decadal changes in snow characteristics in sub-Arctic Sweden, Ambio, 40, 566-74, 2011.

Jones, P. D., Lister, D. H., Osborn, T. J., Harpham, C., Salmon, M. and Morice, C. P.: Hemispheric and large-scale land surface air temperature variations: an extensive revision and an update to 2010, J. Geophys. Res., 117, D05127, doi:10.1029/2011JD017139, 2012.

Kim, Y., Kimball, J. S., McDonald, K. C., and Glassy, J.: Developing a global data record of daily landscape freeze/thaw status using satellite passive microwave remote sensing, IEEE Trans. Geosci. Remote Sens., 49, 949–960, doi:10.1109/TGRS.2010.2070515, 2011.

Langlois, A., Johnson, C. A., Montpetit, B., Royer, A., Blukacz-Richards, E.A., Neave, E., Dolant, C., Roy, A., Arhonditsis, G., Kim, D.-K.F, Kaluskar, S., and Brucker, L.: Detection of rain-on-snow (ROS) events and ice layer formation using passive microwave radiometry: A context for Peary caribou habitat in the Canadian Arctic, Remote Sens. Environ., in review.

Langlois, A., Royer, A., Derksen, C., Montpetit, B., Dupont, F., and Goïta K.: Coupling the snow thermodynamic model SNOWPACK with the microwave emission model of layered snowpacks for subarctic and arctic snow water equivalent retrievals, Water Resour. Res., 48, W12524, doi:10.1029/2012WR012133, 2012.

Liston, G. E. and Hiemstra, C. A.: The Changing Cryosphere: Pan-Arctic Snow Trends (1979–2009), J. Climate, 24, 5691–5712, doi: http://dx.doi.org/10.1175/JCLI-D-11-00081.1, 2011.

Markus, T., Stroeve, J. C., and Miller, J.: Recent changes in Arctic sea ice melt onset, freeze-up, and melt season length, J. Geophys. Res., 114, C12024, doi:10.1029/2009JC005436, 2009.

McBean, G., Alexeev, G., Chen, D., Førland, E., Fyfe, J., Groisman, P. Y., King, R., Melling, H., Vose, R., and Whitfield, P. H.: Arctic climate: past and present, Arctic Climate Impact Assessment, Cambridge, Cambridge University Press, chapter 2, 21–60, 2005.

Nghiem, S. V., Hall, D. K, Foster, J. L., and Neumann, G.: Terrestrial Snow, In: Njoku E. (Ed.) Encyclopedia of Remote Sensing, Springer-Verlag Berlin Heidelberg, 0, doi: 10.1007/SpringerReference_327235, 2014.

Pedersen, S. H., Liston, G. E., Tamstorf, M. P., Westergaard-Nielsen, A., and Schmidt, N. M.: Quantifying Episodic Snowmelt Events in Arctic Ecosystems, Ecosystems, 1-18, 2015.

Rapaic, M., Brown, R., Markovic, M., and Chaumont, D.: An evaluation of temperature and precipitation surface-based and reanalysis datasets for the Canadian Arctic, 1950-2010, Atmos.-Ocean, 53, 283-303, doi:10.1080/07055900.2015.1045825, 2015

Rees, A., Lemmetyinen, J., Derksen, C., Pulliainen, J. and English, M.: Observed and modeled effects of ice lens formation on passive microwave brightness temperatures over snow covered tundra, Remote Sens. Environ., 114, 116–26, 2010.

Rennert, K. J., Roe, G., Putkonen, J., and Bitz, C. M.: Soil thermal and ecological impacts of rain on snow events in the circumpolar Arctic, J. Climate, 22, 2302–15, 2009.

Rienecker, M. M., and Coauthors : MERRA: NASA's Modern-Era Retrospective Analysis for Research and Applications, J. Climate, 24, 3624–3648, doi:10.1175/JCLI-D-11-00015.1, 2011.

Semmens, K. A., Ramage, J., Bartsch, A., and Liston, G. E.: Early snowmelt events: detection, distribution, and significance in a major sub-arctic watershed, Environ. Res. Lett., 8, doi: 10.1088/1748-9326/8/1/014020, 2013.

Serreze, M. C., Barrett, A. P., and Stroeve, J.: Recent changes in tropospheric water vapor over the Arctic as assessed from radiosondes and atmospheric reanalyses, J. Geophys. Res., 117, D10104, doi:10.1029/2011JD017421, 2012.

Stroeve, J., Maslanik, J., and Li, X.: An intercomparison of DMSP F11- and F13-derived sea ice products, Remote Sens. Environ., 64, 132–152, doi:10.1016/S0034-4257(97)00174-0, 1998.

Tedesco, M.: Snowmelt detection over the Greenland ice sheet from SSM/I brightness temperature daily variations, Geophys. Res. Lett., 34, L02504, doi: 10.1029/2006GL028466, 2007.

Tong, J., Dery, S., Jackson, P., and Derksen, C.: Testing snow water equivalent retrieval algorithms for passive microwave remote sensing in an alpine watershed of western Canada, Can. J. Remote Sens., 36(S1), 74–86, 2010.

Trenberth, K. E., Fasullo, J. T., Shepherd, T. G.: Attribution of climate extreme events, Nat. Clim. Chang., 5, 725-730, doi: 10.1038/nclimate2657, 2015.

Wang, L., Wolken, G., Sharp, M., Howell, S., Derksen, C., Brown, R., Markus, T., and Cole, J.: Integrated pan-Arctic melt onset detection from satellite active/passive microwave measurements, 2000–2009, J. Geophys. Res., 116, doi:10.1029/2011JD016256, 2011.

Wang, L., Derksen, C., and Brown, R., and Markus, T.: Recent changes in pan-Arctic melt onset from satellite passive microwave measurements, Geophys. Res. Lett., 40, 522–528, doi:10.1002/grl.50098, 2013.

Wilson, R. R., Bartsch, A., Joly, K., Reynolds, J. H., Orlando, A., and Loya, W. M.: Frequency, timing, extent, and size of winter thaw-refreeze events in Alaska 2001–2008 detected by remotely sensed microwave backscatter data, Polar Biol., doi:10.1007/s00300-012-1272-6, 2012.

Ulaby, F., Moore, R., and Fung, A.: Microwave Remote Sensing: Active and Passive, Vol. 2, Norwood, Massachusetts, Artech House, 1986.

Zhang, X., Vincent, L. A., Hogg, W. D., and Niitsoo, A.: Temperature and precipitation trends in Canada during the 20th century, Atmos.–Ocean, 38, 395–429, doi:10.1080/07055900.2000.9649654, 2000.

Table 1. Data periods for the different satellite passive microwave radiometers used for melt detection in this study.

Satellite	Start Date	End Date	Overpass AM/PM
F-08 SSM/I	Jul 1988	Dec 1991	Ascending/Descending
F-11 SSM/I	Jan 1992	May 1995	Descending/Ascending
F-13 SSM/I	May 1995	Dec 2008	Descending/Ascending
F-17 SSMIS	Jan 2009	present	Descending/Ascending

Table 2. Performance summary of the satellite melt detection using the winter TBD algorithm at snowpit survey sites across Canada, characterized with coincident nearby weather station air temperatures.

Survey Site			Snowpit Feature Depths (cm)			Satellite Melt Detection			Weather Station Air Temperature (℃)					
										Melt Event		Previous 36 HR		Prior Day
Weather Station / Year of Survey	Lat/Lon	Pit Depth	Melt Feature	Height Above Ground	DOY	37V TB AM PM	DOY	Reason for Success/Failure	DOY	# of HRS	Avg. Temp	Avg. Temp	Min. Temp	Max. Temp
Thompson, MB 2005	56.016N 97.260W	53	Melt-freeze crust	9-8	070	**264 260**	**321**	**Rain event / Warm snow**	321	27	0.37	1.35	-4.5	6.8
				45-43		**244 260**	**034**	**Warm snow**	033	8	1.44	-2.69	-5.5	-1.8
Gillam, MB 2005	57.020N 94.140W	63	Melt-freeze crust	53-52.5	070	**232 258**	**034**	**Warm snow**	033	9	0.49	-5.75	-10.5	-2.7
Rae Lakes, NT 2006	63.882N 115.072W	72	Ice layer	36	094	*217 222*	*Not Detected*	*Cold snow*	082	10	3.7	-7.3	-17.9	6.5
			Melt-freeze crust	62										
			Sun crust	72		*209 216*			092	1	1.1	-11.03	-28.3	-1.9
Daring Lake, NT 2007	64.867N 111.573W	48	Ice layer	48-47.5	100	*230 239*	*Not Detected*	*Rain event / Cold snow*	098	2	0.3	-6.47	-13.62	-6.4
Fort McPherson, NT 2008	67.569N 133.618W	54	Ice layer	41 49	097	**243 259**	**093**	**Rain event / Warm Snow**	093	32*	2.9*	-3.57*	-13.0*	6.1*
			Melt-freeze crust	54-53.5		**243 261**	**096**	**Warm Snow**	095	4*	2.88*	-0.83*	-7.5*	4.7*
LaGrande IV, QC 2009	53.648N 73.875W	72	Melt-freeze crust	39.5-39	078	*251 247*	*Not Detected*	*Rain event / Cold snow*	362	5	-0.3	-11.20	-27.7	-6.3
			Ice layer	70-69.5		*251 213*	*Not Detected*	*Rain event / Cold Snow*	076	17	2.45	-19.60	-33.4	-10.6
Churchill, MB 2010	58.7364N 93.8227W	69	Ice layers - multiple	54-45	102	**245 257**	**090**	**Rain event / Warm snow**	090	6**	0.5**	-2.83**	-5.1**	-1.92**
			Melt-freeze/rain crust	69-66		**217 260**	**099**	**Warm snow**	099	13**	5.4**	-1.32**	-9.31**	8.76**

* Indicates that the weather station data is available only during airport business hours (recorded by observer), thus average values are not comparable to other 24 HR stations

** Indicates that air temperatures from a local meteorological station were used instead of the Churchill Climate Station (local met station was closer to the snowpit)

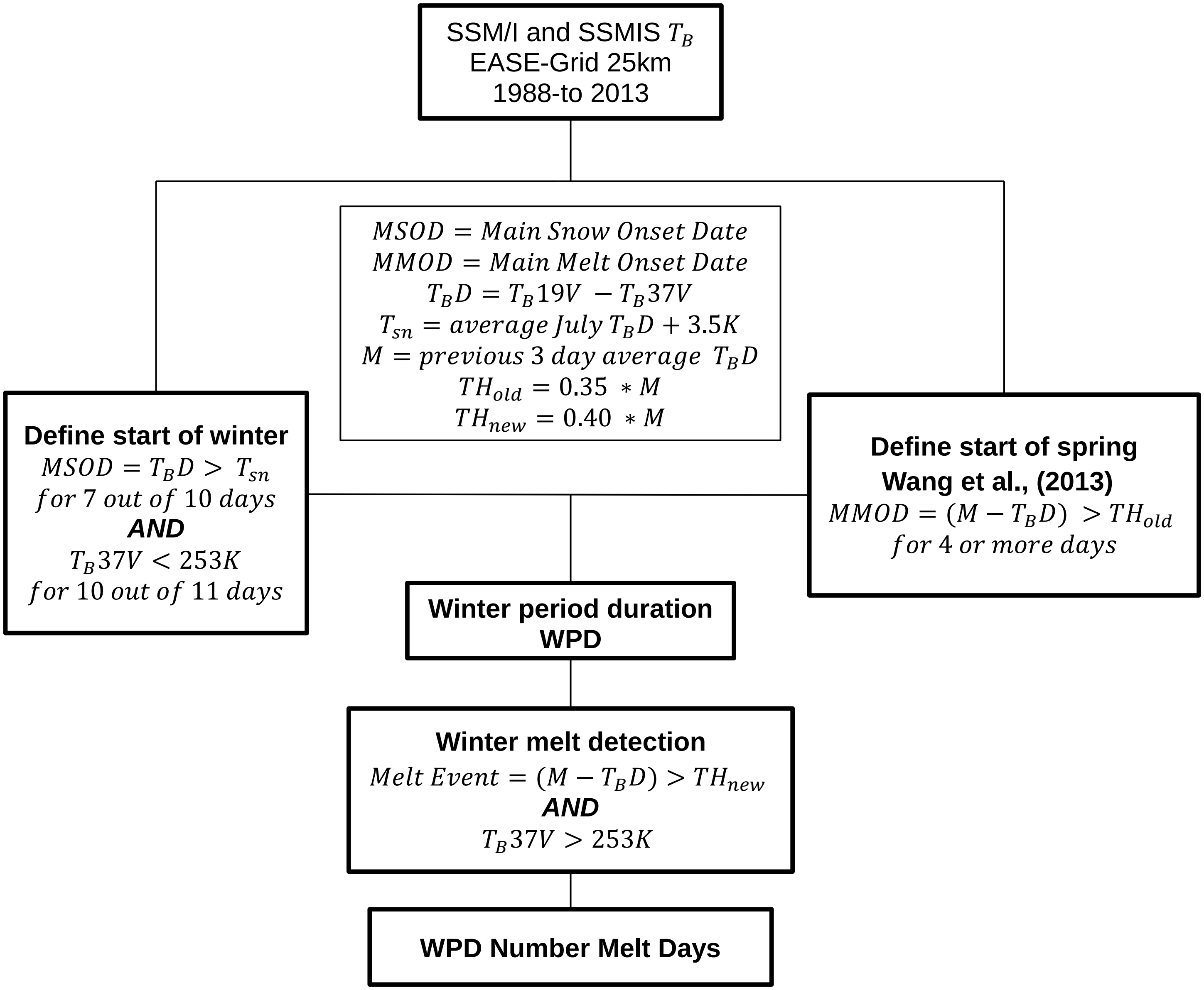

Figure 1. Schematic flow chart of the winter T_BD melt detection method for PMW satellite data.

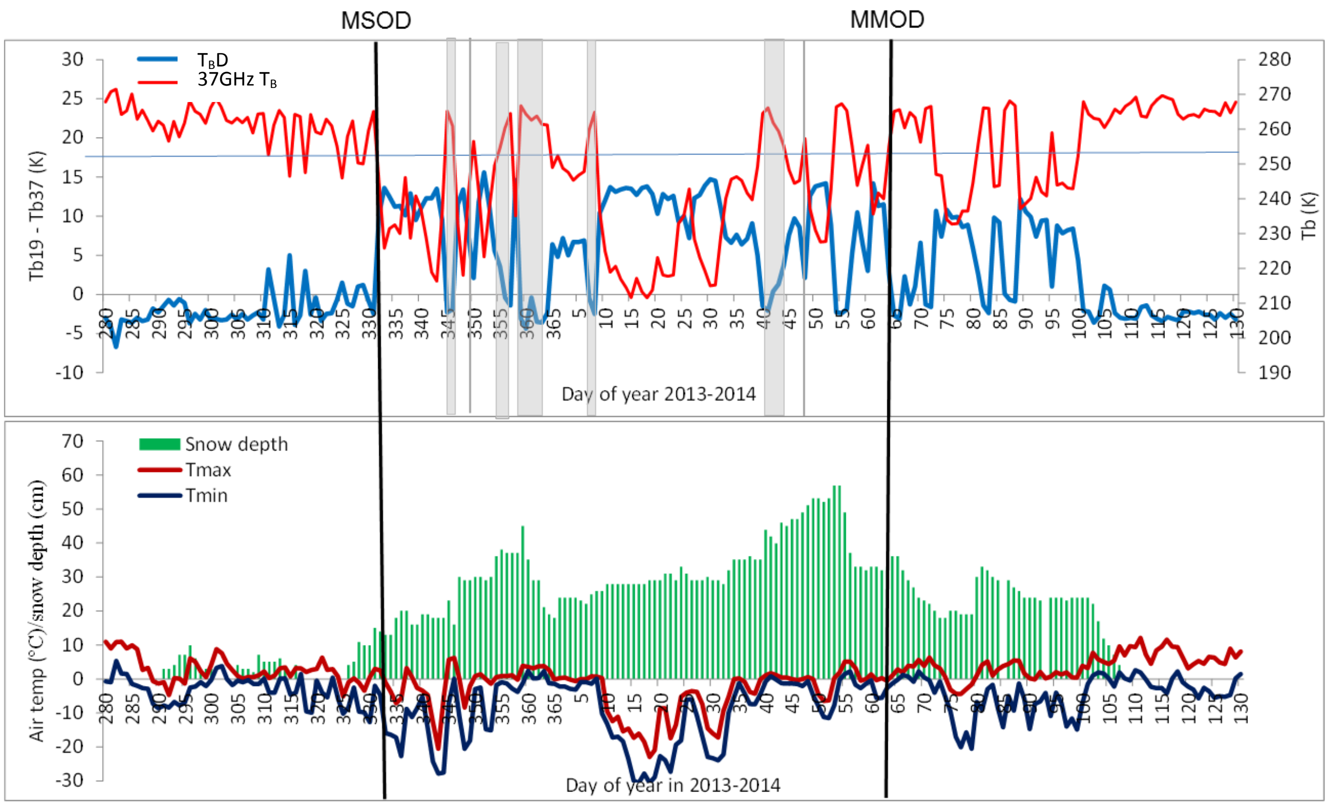

Figure 2. Example of time series of SSM/I T_BD (a) and daily surface air temperature (ºC) /snow depth (cm) (b) at Pudasjarvi, Finland (65.4ºN, 26.97ºE) during the 2013- 2014 winter. The vertical grey lines/bars in (a) represent melt events detected by satellite.

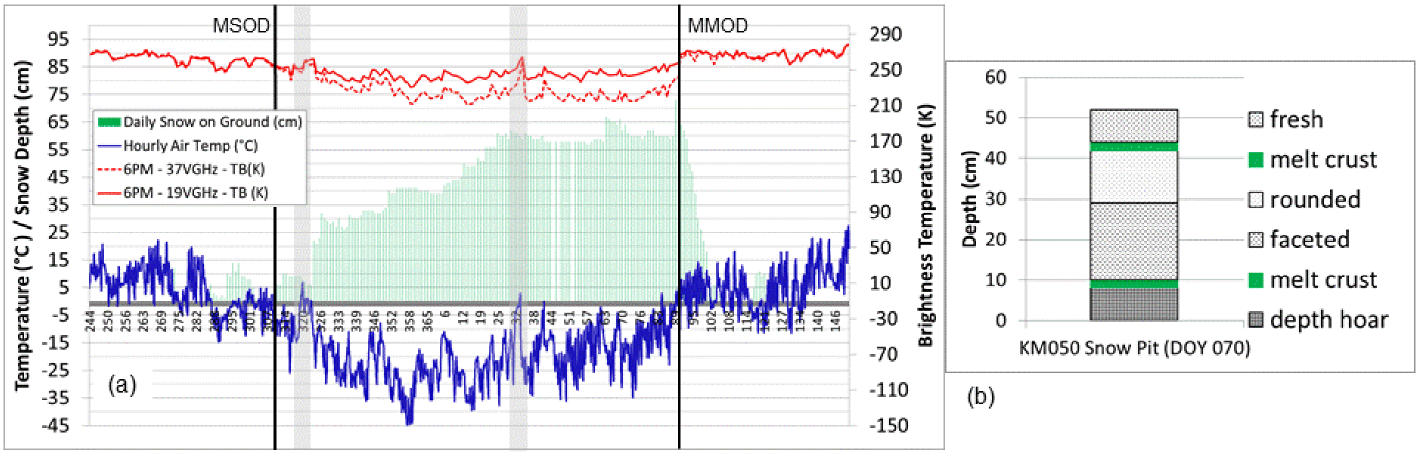

Figure 3. (a) Time series of hourly air temperature and daily snow depth and T_B at the Thompson, Manitoba Meteorological Station from Sep. 2004 to May 2005; the shaded grey bars highlight the timing of the melt events detected by the PMW satellite data. (b) Snow stratigraphy from the KM050 snow pit site surveyed on DOY097. Note that both the early season and recent melt crusts observed in the snowpit agree reasonably well with the timing of two winter melt events recorded at the Thompson airport and detected by the PMW satellite data.

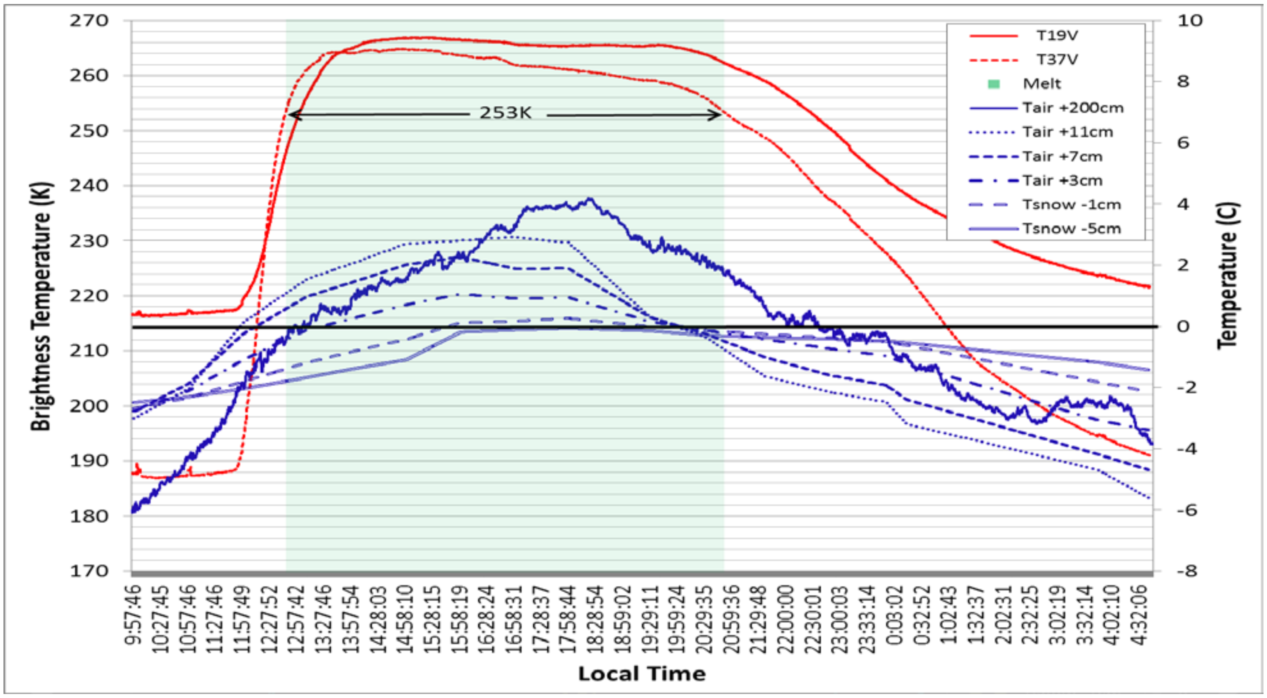

Figure 4. Time series of the surface-based radiometer T_B and the air/snow temperature measurements recorded during April 12-13, 2010 at Churchill MB (58.74º N, 93.82º W). The green shaded region highlights the period when the winter T_BD algorithm successfully detected a winter melt event, the onset of which coincides very closely with the 2 m air temperature sensor.

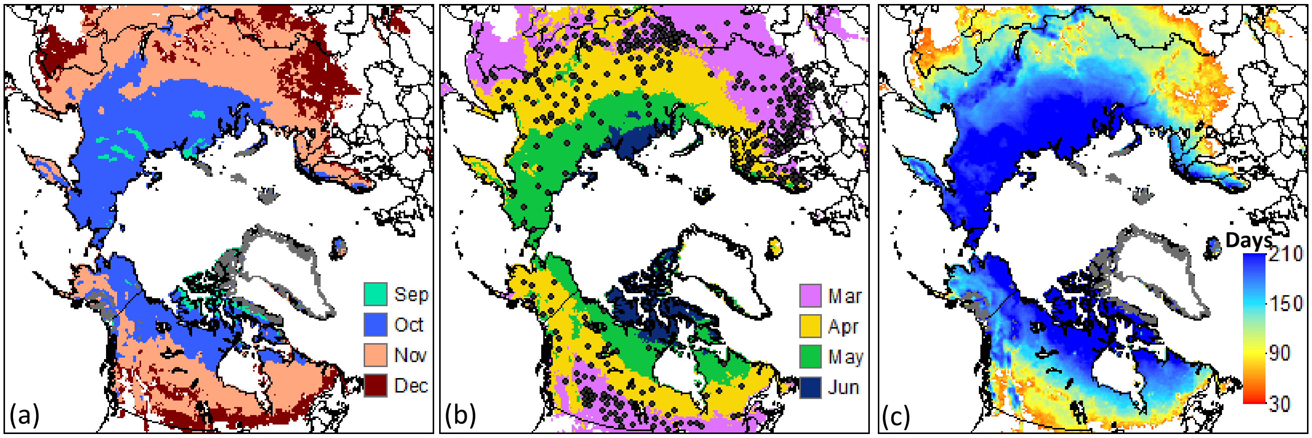

Figure 5. The mean main snow onset date in fall (a), main melt onset date in spring (b), and mean winter period duration (days) (c) during the period 1988-2013. The black dots in (b) represent WMO weather stations used for algorithm development and evaluation.

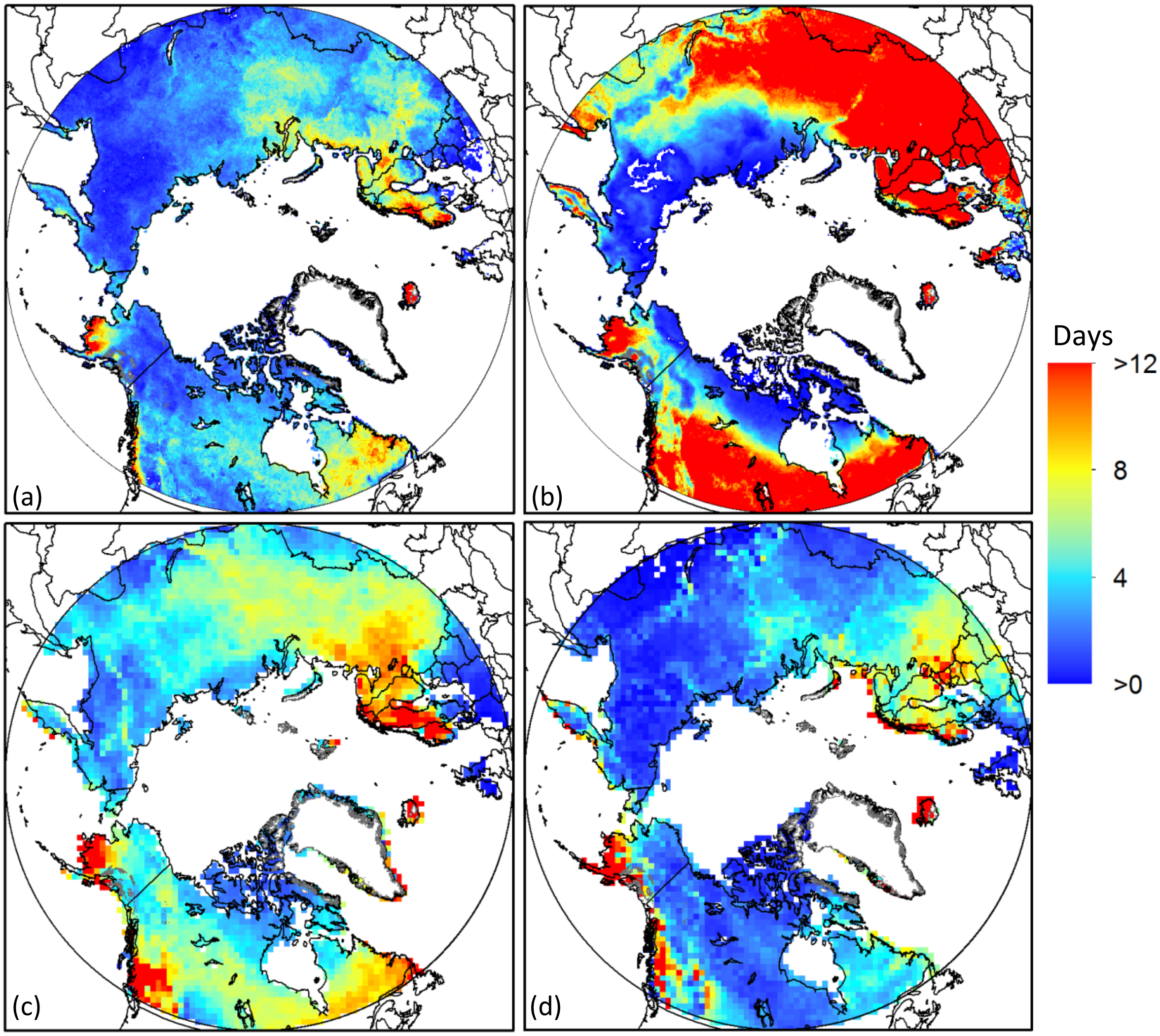

Figure 6. The average annual number of melt days over 1988-2013 from (a) PMW using a varying winter period; (b) PMW using a fixed winter period (November to April); (c) ERA-Interim; and (d) MERRA.

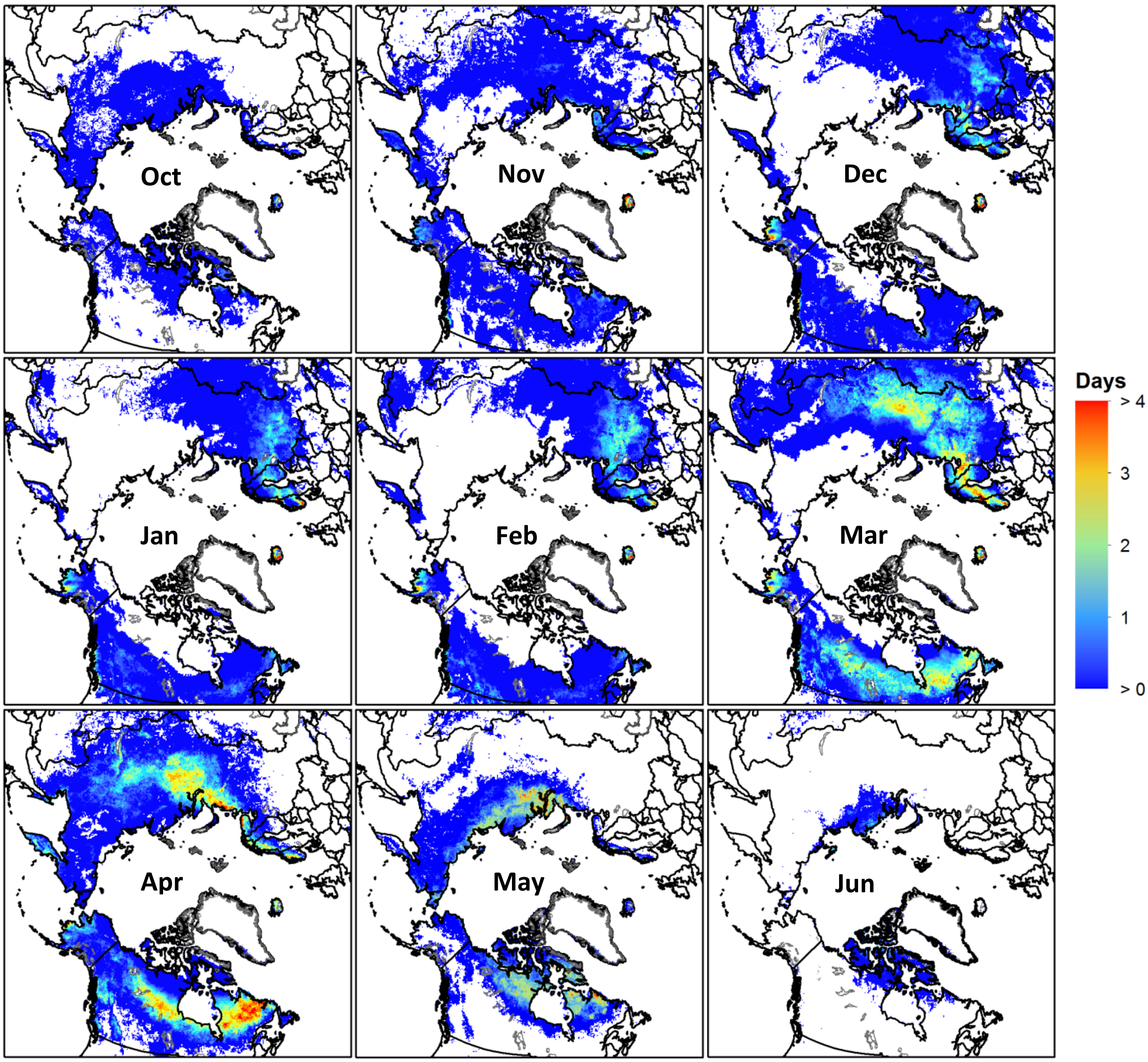

Figure 7. Monthly mean number of melting days from PMW during the period 1988-2013.

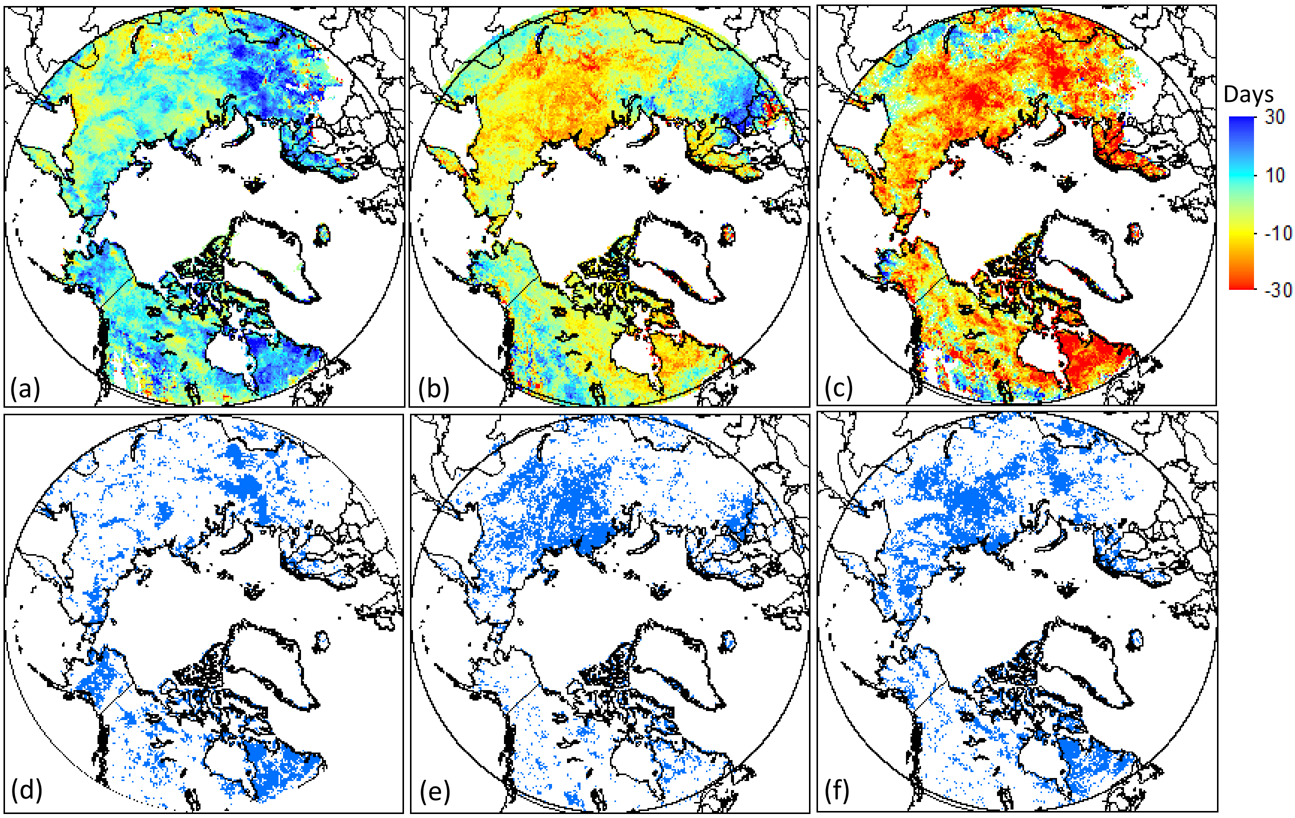

Figure 8. Mann-Kendall trends (days/26yr) over the period 1988-2013 in (a) MSOD, (b) MMOD, (c) WPD. Grid cells with trends statistically significant at the 90% level are shown in (d) MSOD, (e) MMOD, and (f) WPD.

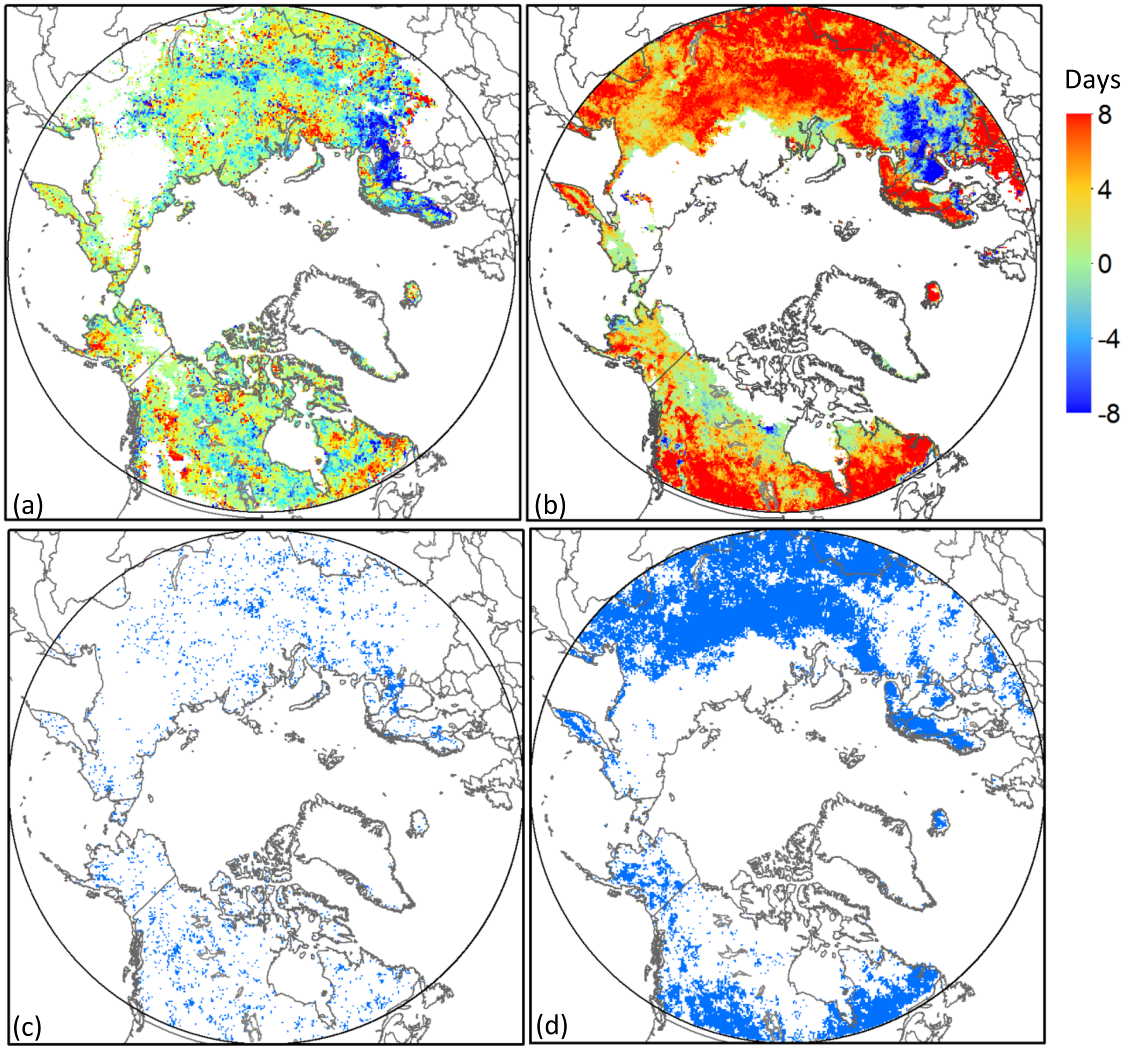

Figure 9. Mann-Kendall trends (days/26yr) over the period 1988-2013 in the number of winter melt days from (a) PMW; (b) PMW-fixed; (c) and (d) show grid cells with trends statistically significant at the 90% level in (a) and (b) respectively.

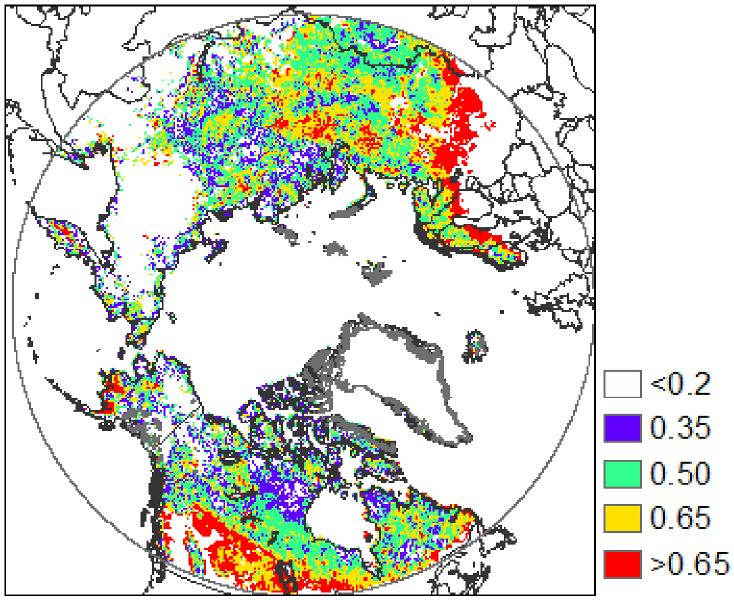

Figure 10. The correlation coefficient between number of melt days and the duration of winter period from PMW during 1988-2013. Correlations greater than 0.35 are statistically significant at 90% confidence level.

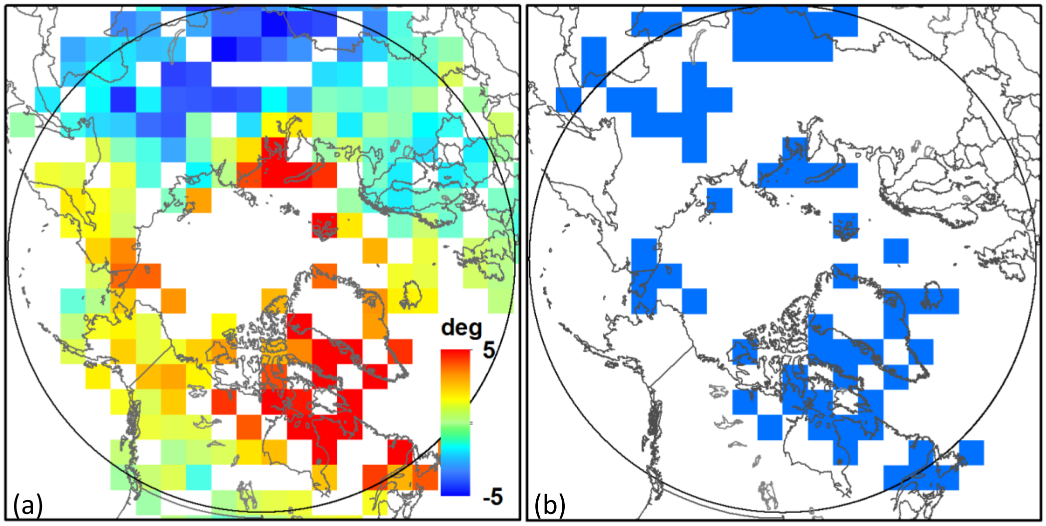

Figure 11. (a) Surface air temperature trends (ºC/26years) during the winter season (DJF) for north of 50º N land areas from CRUTem4 over the period 1988-2013, (b) grid cells with trends statistically significant at the 90% level in (a).

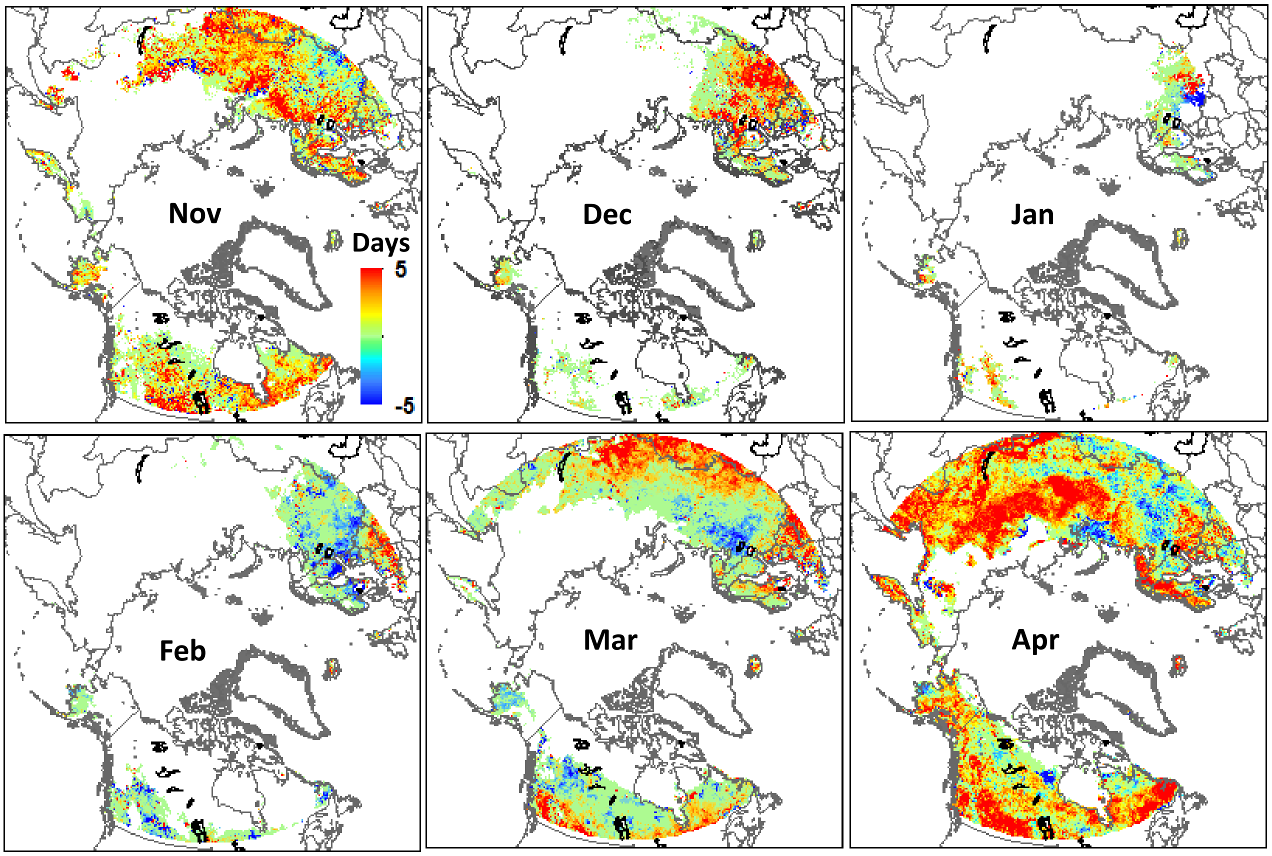

Figure 12. Mann-Kendall trends (days/26yr) in the number of melt days derived by PMW-fixed from November to April during the period 1988-2013.